

Affordable inline structuration measurements of printable mortar with a pocket shear vane

Léo Demont^a, Romain Mesnil^{b,a}, Nicolas Ducoulombier^c, Jean-François Caron^{a,*}

^a*Navier Laboratory, Ecole des Ponts ParisTech, Univ. Gustave Eiffel, CNRS, Marne-La-Vallée, France*

^b*Build'In, École des Ponts ParisTech, Marne-La-Vallée, France*

^c*XtreeE, 18 Rue du Jura, 94150 Rungis*

Abstract

The control of mortar rheology is of paramount importance in the design of systems and structures in 3D printing concrete by extrusion. This is particularly sensitive for two-component (2K) processes that use an accelerator to switch the printed mortar very quickly from a liquid behavior to a sufficiently solid behavior to be able to be printed. It is necessary to set up simple and effective tests within a precise methodological framework to qualify materials evolving so quickly in an industrial context. It is obvious that inline solutions, that is to say, post-printing solutions, will be more desirable than benchtop-type solutions reproducing the printing conditions as well as possible, but imperfectly. After some main key points about measuring the structuration of mortars, we propose an original inline test using a pocket shear vane tester. The protocols are precisely described and the simplicity and quality of the results are demonstrated.

Keywords: additive manufacturing, concrete 3D printing, pocket shear vane, yield stress, build-up rate, inline measurement

1. Introduction

The control of mortar rheology is of paramount importance in the design of systems and structures in 3D printing concrete by extrusion. The main rheological requirements for a successful implementation of the process are detailed in a seminal paper by Roussel [1], where the importance of yield stress evolution is illustrated with the analytical solution of a vertical wall. The *buildability requirement* states that the stress resulting from self-weight ρg does not exceed the yield stress τ_c of the material, as shown in equation (1) and in Figure 1,

*Corresponding author
Email: jean-francois.caron@enpc.fr

where it is assumed that the total height $H(t)$ is a linear function of time.

$$\tau_{cr}(t) > \frac{\rho g H(t)}{\sqrt{3}} \quad (1)$$

If the build-up rate (or structuration) is not sufficient, the limit of constructability is reached (red zone in Figure 1) and printing is no longer possible because the first layers cannot support the load of the successive ones. Moreover, a rapid build-up rate (or structuration) is then required to increase productivity. For example, one gets $A_{thix} \simeq 25 \text{ Pa/s}$ (from Eq. (4)) for a vertical speed $V_r = 6 \text{ m/hour}$. As a result, the yield stress of a printable material spans several decades during the first hours of printing [2]. The build-up rate is also important in the context of the fiber-reinforced printed mortars, the impregnation of the fibers will be better ensured by a fluid material, which then quickly structures itself (see for example the process *Flow-Based Pultrusion* [3][4][5] for more details). More recently, Carneau and coauthors proposed a stability criterion based on the structuration rate for the layer-pressing problem and showed that local layer geometry may be impacted by its value [6].

1.1. Rheological behavior of printable mortars

As a general rule, the evolution of mortar or any traditional cementitious paste rheological properties can be separated into two stages: the dormant period which generally corresponds to a printable mortar to the first hour after it has been mixed, which we will call the very young age, then the setting time characterized by an exponential acceleration of the hydration reactions and therefore of the structuration, as shown in [7].

For the dormant period, Roussel proposed a linear evolution of the yield stress (Eq. 2) in [8], which captures well the very young age behavior.

$$\tau_{cr}(t) = \tau_0 + t \cdot A_{thix} \quad (2)$$

Perrot *et al.* proposed a nonlinear model for the time evolution of yield stress, with the introduction of a characteristic time t_c [9], shown in equation (3). The merit of this model is to converge towards an exponential model for a large time, thus capturing hydration, but it also allows fixing the slope at ($t = 0$).

$$\tau_{cr}(t) = A_{thix} t_c \left(e^{t/t_c} - 1 \right) + \tau_0 \quad (3)$$

Note that these equations hold only after the re-flocculation phase that occurs just after the material is set to rest, and that other researchers observe a re-flocculation rate much higher than the structuration rate [10].

Assuming a linear evolution of the yield stress over time, the build-up rate requirement can thus be written as follows, assuming a constant vertical speed V_z and vertical printed walls.

$$\tau_0 + \left(A_{thix} - \frac{\rho g V_z}{\sqrt{3}} \right) t > 0 \quad (4)$$

If one neglects the initial yield stress, which is usually low in the context of bi-component (2K) concrete 3D printing, the buildability requirements just write $\left(A_{thix} - \frac{\rho g V_z}{\sqrt{3}}\right) > 0$. In other words, the maximal vertical speed is directly proportional to the structuration rate A_{thix} .

In the bi-component (2K) technology, such as the one developed by XtremE and used in the Build'in platform, the mortar has a low yield stress that is nearly constant over time (A_{thix} is small) to efficiently handle the pumping stage, even for high plastic viscosity mortar such as UHPC. Then, the increase of rheological properties is started (A_{thix} increasing) through the addition of an accelerator using a dosing and mixing device located in the printing head just before extrusion [11, 12, 13]. The schematic evolution of rheological properties over time of such a process is illustrated in Figure 1. With the use of an appropriate additive dosing, the material timeline (continuous blue curve) has a suitable build-up rate A_{thix} that allows respecting the buildability limit (Eq. 1) shown in red. On the contrary, insufficient dosing means an insufficient build-up: the material timeline (dashed blue curve) goes below the buildability limit and fails by plastic flow as shown in the pictogram. Different accelerators for 3D printing concrete exist in the literature, but in this work, an alkali-free aluminum sulfate solution is used. From a physicochemical point of view, the addition of alkali-free additives triggers the rapid formation of ettringite needles, due to the reaction between aluminum sulfate and calcium [14]. Those needles jam the internal mortar microstructure which results in an increase in yield stress over time.

Dressler and coauthors showed that the accelerator concentration had a significant impact on the early-age structuration of printable mortar [15]. However, the effect of the accelerator dosage on the build-up rate is still an active topic of research, as the description of the interaction between plasticizer, accelerator, cement, and the compactness of the granular skeleton [16] needs to be clarified. However, note that this type of accelerator does not necessarily reduce the dormant period, after which occurs the classic hydration phenomena leading to the acceleration of the CSH formation, which usually happens seven hours after mixing with water in our case. The development of systematic and representative inline characterization methods of the printed material is thus necessary. In this paper, we will then restrict our analysis to this linear increase of yield stress through time and assume that the addition of accelerator is only increasing the slope of the linear increase of the yield stress over time A_{thix} , which simplifies the analytical derivation.

1.2. Measuring build-up rate

Several methods for measuring the build-up rate have been proposed for printing mortars [13], but the question arises whether they are applicable in the form of systematic control tests at a very young age representative of the true two-component printing process.

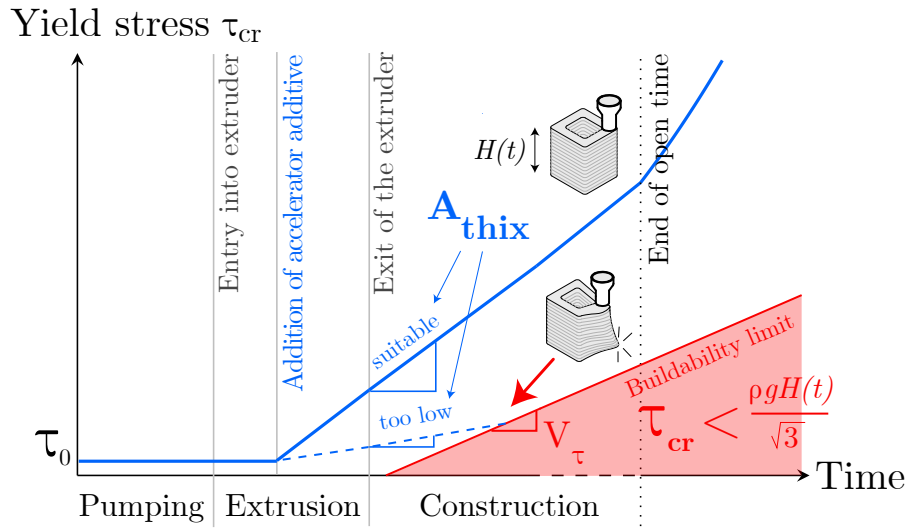


Figure 1: Evolution of shear threshold τ_{cr} of a 2K printed material.

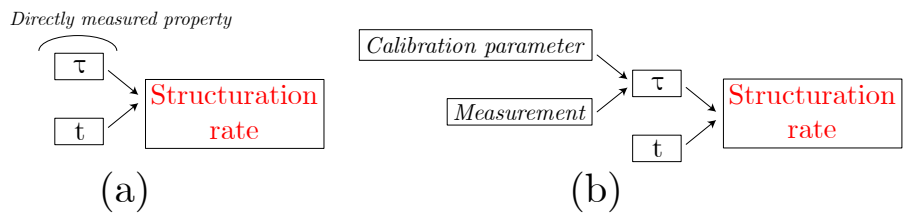


Figure 2: Diagram of the principles of direct (a) and indirect (b) measurement of the structuration rate.

The fast evolution of yield stress makes characterization difficult. Promising methods that can measure the yield stress of printable materials can be found in [2, 17]. We will focus here on so-called direct or destructive techniques (Figure 2a). With these, the time evolution of the yield stress τ_{cr} associated with rupture or the onset of flow, is obtained via one or several measurements. We, therefore, do not discuss indirect techniques, such as ultrasound measurements, where the threshold τ_{cr} is calculated as a function of a material property p and rheological data c specific to the material and obtained by another direct test [18] (Figure 2b), nor non-destructive mechanical measurements, such as static Vicat plate or needle tests [19][20] which do not directly measure the yield stress (or rupture) related to the collapse of the internal granular system. In the next section, we review and precise some specific and important aspects which qualify a given test protocol. After that, we will introduce and detail the pocket hand vane test proposal.

2. Principal methods and some key points for structuration rate measurements.

We highlight here some important points for the qualification of a test aiming to measure the build-up rate of a mortar. Some definitions are given to help define the limitations of a given test. A rheological test can be characterized by several steps:

- A sample of volume Ω is prepared, ideally by using a material that has been pumped by the extrusion process, in a time t_{sample}
- After a sufficient time t_{rest} , for dispersing the accelerators and for the structuration to be initiated at the moment of the measurement [8][21], the test phase can begin, and τ_0 is the initial threshold at this instant.
- The test is prepared, for example by putting the material sample on a testing machine, and performed, which requires at least the time t_{min}

If one considers inline process, the time t_{sample} necessary for preparation is simply equal to Ω/Q , where Q is the flow-rate of the extruder: it is thus system dependent and is not an intrinsic property of the test. The flow rate may vary significantly depending on the process. A good bulk approximation sets Q between 1 – 10L/min for many 3d printing processes. In addition, every test can measure the yield stress between two bounds $[\tau_{min}, \tau_{max}]$.

Table 1 displays the characteristics for some popular tests listed in [22]. Some tests are *gravity-driven*, like the slug-test [23], Abrams cone, or mini-cone. Other are *gravity-dependent*, like the compression test. It shall be noted that the slug-test is by design a test with no rest time. It is also the only test where the notion of preparation time t_{sample} is not relevant since the material tested is always the material at the nozzle exit.

The following of this section discusses some aspects to consider when handling materials with a fast structuration.

Test	Gravity dependent	τ_{min}	τ_{max}	H [mm]	Ω [l]	t_{rest} [s]	t_{min} [s]
Unconfined compression	yes	$\frac{\rho g H}{\sqrt{3}}$	-	140	0.54	10 – 100	1 – 10
Slug test	yes	$\sqrt{\frac{\rho g \mu_p V}{1.074}}$	-	$\frac{\tau D \sqrt{3}}{\rho g}$	$\frac{S \tau D \sqrt{3}}{\rho g}$	0	$\frac{\Omega}{Q}$
Abrams cone	yes	-	$\frac{\rho g H}{\sqrt{3}}$	304	5.5	60	1 – 10
Mini cone penetrometry	yes	-	$\frac{\rho g H}{\sqrt{3}}$	150	0.67	60	1 – 10
penetrometry	no	-	-	-	$\simeq 1$	10 – 100	-

Table 1: Popular tests for yield stress evaluation and their characteristics. Dashes indicate machine-dependent parameters.

2.1. Serial versus continuous measurement

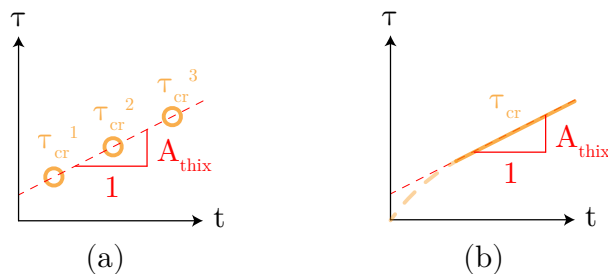


Figure 3: Diagram of principles of serial (a) and continuous (b) measurement of the structuration rate, assumed linear at an early age and described by a single parameter A_{thix} .

The structuration rate is measured through two distinct approaches. The first one consists in carrying out a serial measurement, i.e. a series of measurements of the yield stress (τ_{cr}^n) at different ages t_n and on distinct samples (Figure 3a). In the case of cement mortars and yield stress fluids in general, these measurements can be carried out without a rheometer, thanks to practical techniques whose principle is to trigger the material flow or rupture by destructive mechanical stress. Many so-called workability tests, which aim to qualify the flow properties of concrete empirically, are based on this principle [24] but only some allow to measure yield stress using appropriate physical modeling. The Abrams cone test uses a model proposed in [25] and there are also techniques from soil mechanics (shear box [26], rapid indentation) or from industry (squeeze test [27] also called *squeezing test*) which provide satisfactory measurements of mortars and cementitious pastes yield stress. Vane shear test can also be used for the evaluation of yield stress of 3d printing mortars [28]. The second approach, called continuous, consists in continuously characterizing τ_{cr} by a single measurement extended over time (Figure 3b) and carried out on a single sample. Slow penetrometry (review in [17]) corresponds to this typology. The two approaches have their merits: the serial measurements only

provide snapshots of the material properties, but they may be easier to replicate on several samples and provide thus statistical information such as confidence intervals or might give access to mix homogeneity. Continuous measurements provide more granularity, but usually rely on more expensive equipment and are done once, thus preventing statistical analysis.

2.2. Benchtop versus inline measurement

The characterization of the build-up rate can be carried out on the bench or inline, i.e. either beforehand by producing the material and carrying tests with generic laboratory equipment, or directly during printing.

The benchtop measurements have the advantage of being reproducible with simple tools (table mixer, balance...) but do not guarantee that the studied material is exactly the one printed, as shown in this paper. The inline test can be realized more easily on the very new printed mortar and can be realized many times at the same state of structuration because the accelerated material is produced continuously. Moreover, it has the great advantage to characterize the material that has gone through the same history of solicitation as the actual printed material. From the previous review, we can conclude that in situ easy-to-perform tests and corresponding methodology needs to be developed to measure efficiently the yield stress at different time frame using apparatus that can cover many decades to measure the build-up rate of the material and be able to set properly the printing parameter during a printing session. The next subsections precise some last definitions.

2.3. Measurement window

Material tests usually have a specific operating domain and can measure values of yield stresses τ_{cr} within a window $[\tau_{min}, \tau_{max}]$. When the build-up rate is high, the time interval $[t_{max} - t_{min}]$ during which the series of tests can be carried out, later called *measurement window*, is generally small.

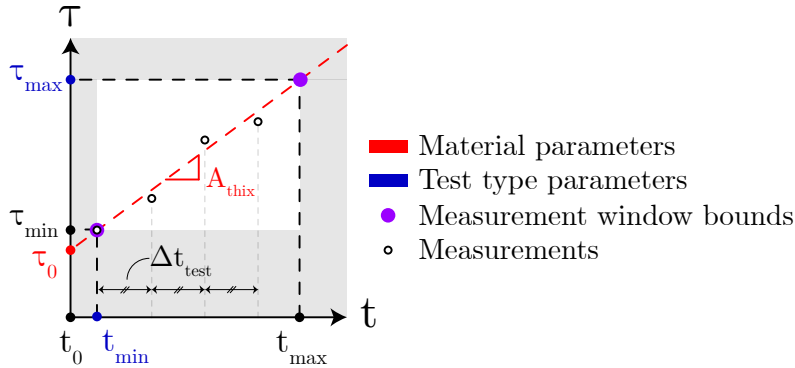


Figure 4: Graph illustrating measurement window bounded by the points (t_{min}, τ_{min}) and (t_{max}, τ_{max}) .

Figure 4 illustrates a typical measurement window and highlights that some parameters depend on the material, A_{thix} and τ_0 , and others, t_{min} , τ_{max} depend on the test type. For a two-component 3D printing, large A_{thix} reduces drastically t_{max} and thus the size of the measurement window.

2.4. Number of possible tests inside the measurement window

Another important point is to anticipate how many tests are possible inside the measurement windows. Considering, that measuring A_{thix} by a linear regression requires n trials, at least $n = 3$, and Δt_{test} the delay between 2 successive measurements, the number n of possible tests verifies the following inequality (Eq. 5):

$$t_{max} - t_{min} \geq n \cdot \Delta t_{test} \quad (5)$$

The spacing delay between trials Δt_{test} will be at least equal to t_{min} , which corresponds to the duration of the test. However, depending on the precision δ_τ of the type of test, it may be necessary to increase this delay because Δt_{test} must be large enough to be able to obtain sufficiently contrasted measurements. From Eq.2, the uncertainty/structuration rate ratio $\frac{\delta_\tau}{A_{thix}}$ gives a minimum value for Δt_{test} :

$$\Delta t_{test} \geq \frac{\delta_\tau}{A_{thix}} \quad (6)$$

2.5. Homogeneity

The homogeneity of the material across the tested sample is another significant aspect to keep in mind designing a test. When the material has a rapid structuration, the yield stress evolves during the preparation of the sample. From Eq.2, we write $\Delta\tau_{cr}$ the variation of yield stress across the sample during t_{sample} .

$$\Delta\tau_{cr} \sim A_{thix} \cdot t_{sample} = \frac{A_{thix}\Omega}{Q} \quad (7)$$

The material is tested after a given time t^* . A necessary condition for material homogeneity is that the variation of yield stress across the sample remains small compared to the measured yield stress:

$$\frac{\Delta\tau_{cr}}{\tau_{cr}(t^*)} = \frac{A_{thix} \cdot t_{sample}}{A_{thix} \cdot t^* + \tau_0} = \frac{t_{sample}}{t^* + \frac{\tau_0}{A_{thix}}} \ll 1$$

Introducing $t_{thix} = \tau_0/A_{thix}$ which is a characteristic time of the material, corresponding (see Eq.2) to the time need for the material to double its initial yield stress, the condition for a good homogeneity is (8):

$$t^* \gg t_{sample} - t_{thix} \quad (8)$$

Having in mind these different parameters and constraints regarding window measurement size, number of possible tests, and homogeneity conditions, we propose in the following, original method using a so-called pocket hand vane test. The device, the methodology, and the first results are detailed.

3. Pocket hand vane presentation and mechanical analysis

The principle of the vane test (or scissometer) is to shear a sample of material by applying a torque to it while measuring the stress necessary to trigger its flow or its rupture. Just like the cone test, it prescribes a perfectly known stress field, here a pure shear. This type of measurement on a bench with an immersed vane, mobilizing fairly large quantities of mortar is classic [29] (Figure 5b) to measure the shear yield stress [30] and structuration rate [31] of cementitious materials dedicated to casting, and the results obtained can be accurately correlated with a rheometer [32].

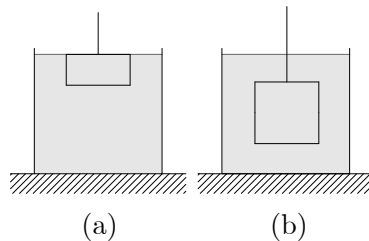


Figure 5: Diagram of the measurement area with a pocket vane (a) and the classic vane (b).

3.1. The pocket vane

The pocket vane (also called *Torvane*) is a smaller version of the scissometer, except that the vane is positioned on the surface of the specimen (Figure 5a). Initially developed for fine-grained soils [29], it has never been used, to our knowledge, on cementitious materials. Like a hand vane, it has a knurled head that is manually turned and connected to a vane shaft. But, the loading (i.e. shear stress proportional to the torque) is localized in the first few millimeters at the surface of the specimen. The exerted stress value can be related to the value of the torque given by the graduations on the apparatus head, thanks to the analysis made in the next section.

3.2. Mechanical analysis

The mechanical analysis was initially proposed for the determination of undrained cohesion of clays studied in geotechnics [33] and considers that the flow stress is exerted on a cylinder inscribed around the blades. Indeed it has been shown that at the moment of flow, the cylinder of material embedded in the blades rotates like a rigid body. The flow is located uniformly along a thin

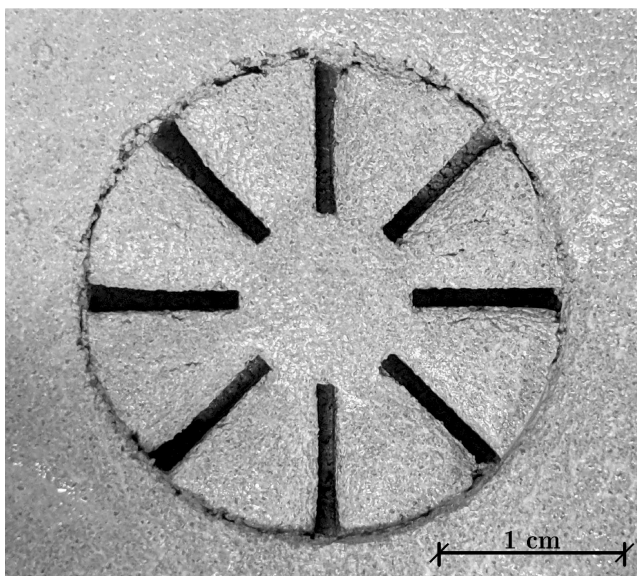


Figure 6: The test area of a printable mortar tested with a pocket vane with the Standard vane head at a very young age. The imprint of the vanes and the cylindrical rupture is clearly visible.

cylindrical layer near the tips of the blades [34], clearly visible in Figure 6 . For a classic scissometer, the measured torque T_{cr} is due to two components, one resulting from the shear on the lateral curved edge T_s and the other $2T_e$ from the shear on the two upper and lower horizontal edges of the inscribed cylinder [35] [36]:

$$T_{cr} = T_s + 2T_e \quad (9)$$

The case of the pocket shear vane is different. The blades are inserted at the surface so there is only one sheared horizontal edge:

$$T_{cr} = T_s + T_e \quad (10)$$

These differences are illustrated in Figure 7. T_s is given by :

$$T_s = (\pi DH) \frac{D}{2} \tau_s \quad (11)$$

where πDH represents the curved surface of the cylinder, with D the diameter of the cylinder, H its height, and $\frac{D}{2}$ the lever arm.

$\tau_e(r)$ is not known a priori, probably linear in r , and the balance of the torque exerted during the flow 12 is:

$$T_{cr} = (\pi DH) \frac{D}{2} \tau_s + 2\pi \int_0^{D/2} \tau_e(r) r^2 dr \quad (12)$$

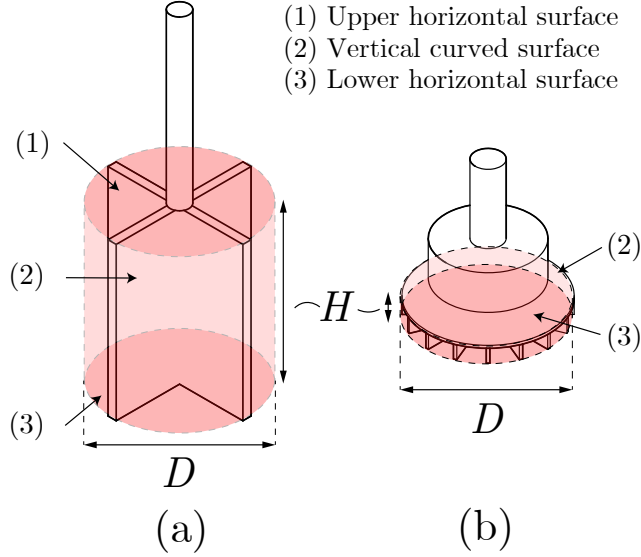


Figure 7: Diagram of sheared surfaces with a classic vane (a) and a pocket vane (b).

At the time of the flow, it is assumed that the constraints τ_s and τ_e are uniform and equal to τ_{cr} . In this case, the Equation 9 is reduced to a simpler form where we can directly express T_{cr} according to the dimensions of the blades and τ_{cr} :

$$T_{cr} = \frac{\pi D^3 \tau_{cr}}{12} \left(1 + \frac{6H}{D} \right) \quad (13)$$

It is noteworthy that the test prescribes a pure shear stress state, with a negligible elongational or compressive component, unlike other types of tests (penetrometry, Abrams cone test).

4. Material and protocols

We define now the used material and the protocols for the different experimentations that we carry out, benchtop and inline experimentations.

4.1. Material and preparation

In this study, the mortar is formulated using the 3DPG dry mix provided by Lafarge. The maximum particle size of this dry mix is $\phi_{max} = 0.8\text{mm}$. The water (including the superplasticizer water) to powder mass ratio is equal to $\frac{E}{P} = 0.1$. The phosphonates base superplasticizer is adjusted to reach an initial yield stress comprised between 100 and 200 Pa. The resulting superplasticizer quantity is usually comprised between 0.5% and 0.6% of the dry mix mass. Then, an aluminum sulfate-based accelerator Floquat ASL is added varying

the dosage between 1.5g/kg and 17g/kg (1 and 17 mL/kg) to obtain different build-up rates.

The mixing process is either made using a benchtop mixing unit, the Hobart HSM10 mixer, or the mixing unit of the XtreeE printing cell.

For both production the mixing protocol is the following:

- a) the superplasticizer and the water are weighted and mixed in one container
- b) The dry mix is weighted and introduced in the mixing unit
- c) The mixing unit is started (at low speed for the benchtop unit) and the liquids are slowly poured for approximately 1 min.
- d) the mixing is continued for 5 more minutes (at high speed when using the benchtop unit)

Concerning the accelerator, for the benchtop it is added and dispersed following this protocol:

- a) the accelerator solution is weighted in a small recipient
- b) the mixing unit is started at a large speed
- c) the accelerator is poured quickly and the chronometer is started (t=0)
- d) The mixing is continued for 30 more seconds

For the inline test, the accelerator is added through the printing head via a dosing micro-pump and following the XtreeE process.

After the end of the acceleration protocol, the accelerated mortar is for both tests (benchtop and inline), poured into containers with different sizes (see Figure 9). In the following, *ex-situ* tests refer to these tests realized in containers. Note that the free surface of the container needs to be as smooth as possible by tapping by hand or using a spatula. This facilitates the insertion of the scissometers into the material.

For the inline situation, dedicated printing laces are also carried out for direct *in-situ* tests.

The build-up rate measurements use the devices and protocols described in the next section.

4.2. Tests protocols

The pocket vane used in this paper is the Humboldt H-4212MH that refers to the ASTM D8121/D8121M standard [29].

Three interchangeable vane heads are available, which are chosen according to the strength range of the studied material and give access to different decades of yield stress values. The data are presented in Table 2. The measuring range increases as the diameter of the sheared surface D decreases. The blade height H is constant, 5.2 mm. The maximum torque applicable using the instrument corresponds to a complete rotation of the head (10 graduations). The change in

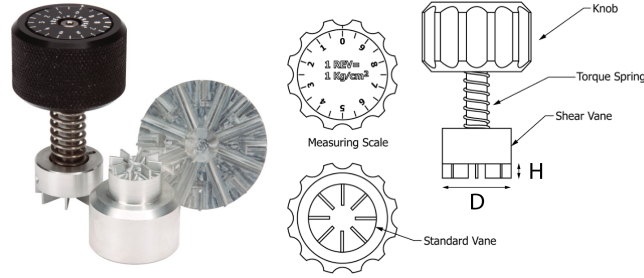


Figure 8: Left : a pocket shear vane *Humboldt H-4212MH*, right : schematic from ASTM D8121/D8121M standard [29].

Vane head	D (mm)	$[\tau_{min}, \tau_{max}]$ (kPa)	δ_{τ} (kPa)
Sensitive	47.5	1 - 20	1
Standard	25.5	5 - 100	5
Large Capacity	19	12.5 - 250	12.5

Table 2: Data relating to the different vane heads of the pocket shear vane. D : Diameter of the sheared surface, $[\tau_{min}, \tau_{max}]$: Yield stress measurement domain (kPa), δ_{τ} : Accuracy of the graduation.

diameter of the blades has a limited influence on the measurement of fine-grained soils [35], this will be discussed later in this article.

The yield stress evolution is then measured using this apparatus and the appropriate vane geometry. The vanes are inserted in the samples and tests are carried out by turning each vane at a constant low speed (approximately 3 rpm) until peak stress is reached.

4.2.1. Ex-situ benchtop and ex-situ inline tests

For the ex-situ tests the scissometers or footprints are placed following the arrangement shown in Figure 9 c. The footprint refers to a plastic model of the different vane geometry made by FDM 3D printing process. Inserted just after the container is filled, when the mortar is still fresh, they may help to introduce the vane head for testing without damaging it. These footprints are replaced with the real vane apparatus just before testing. Sets of 3 tests are carried out to obtain an average value and dispersion estimation at each time and each corresponding yield stress value. By rotating $\pi/3$, it is thus possible to successively carry out 2 sets of 3 tests per container: the first set with the sensitive vane head for a very young material, and the second one with the standard vane head for a more structured material (see Figure 10).

4.2.2. In-situ inline tests

For in-situ inline tests, meaning direct tests on printed laces, the protocol is almost the same, but directly along the top of the printed wall (fig.11).

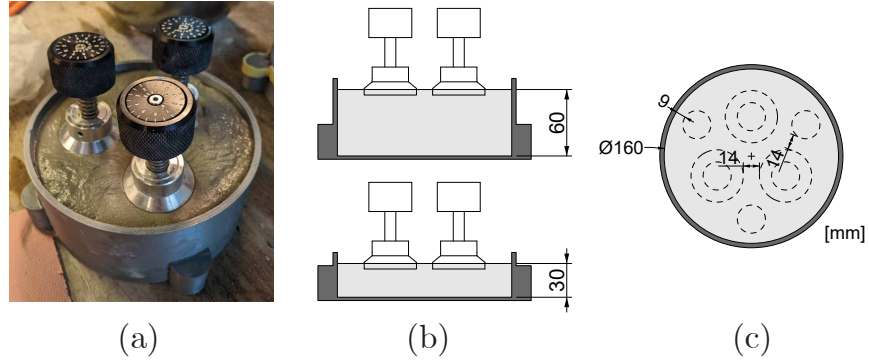


Figure 9: The ex-situ measuring device with three pocket scissometers, (b) two container heights are tested, (c) top view of the container and position of the 2 sets of 3 tests in dotted line.

The Standard vane is chosen (diameter 25.5 mm) and the lace width is set to be around 30 mm, a common value with our system. To avoid any edge effect, the vanes will be arranged according to the diagram shown in Figure 11. The yield stress is also measured at different resting times for similar accelerator content as for the ex-situ inline test.

5. Preliminary tests

In this section, preliminary tests are investigated to judge the relevance of the proposal.

5.1. Comparison of classical and pocket scissometer benchtop measurements

To validate the tool and the operating mode, first benchtop experiments are carried out. A comparison between the yield stress measurements made using a standard hand vane (Figure 12), usually used by the company *XtreeE* and already qualified by the community for yield stress measurement, and the pocket hand vane, are made. In this case, the accelerator dosage was chosen equal to 7.5g/kg of dry mix.

The vane measurements are made on numerous prismatic containers filled after the dispersion of the accelerator in the benchtop mixing unit. After given resting times, the hand vanes are inserted inside the tested specimen and slowly rotated at a similar speed (≈ 3 rpm). The results are reported in Figure 13 and are comparable, which assesses the correct precision of the absolute yield stress measured value. Moreover, the evolution measured by both apparatus is also really similar which demonstrates, first the assumed linear evolution (Eq.2), and the potential of the pocket vane geometry to measure the build-up rate of fine-grained printable materials.

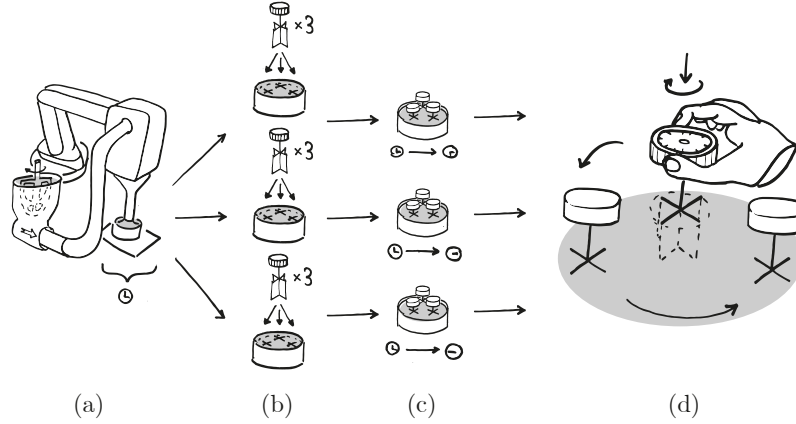


Figure 10: Illustration of the steps of an ex-situ inline vane test: (a) Preparation of the sample: filling a container with the printed material (b) Inserting the vanes or footprints (c) Waiting for a given amount of time (d) Performing sets of three tests for each sample.

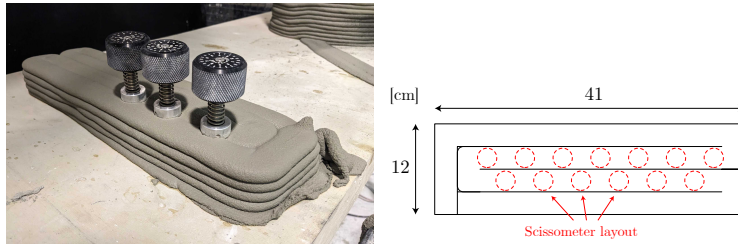


Figure 11: Illustration of an in-situ inline vane test : Left: a printed sample dedicated to the lace measurement. Right: Layout of vanes on the printed sample.

5.2. First campaign of benchtop measurements using a pocket scissometer

A series of benchtop experiments are carried out to estimate better the accuracy that can be expected from the pocket vane and verify the hypothesis taken in the theoretical analysis. A total of 10 series were carried out for increasing dosages of accelerator D_{acc} (9, 13, 17 g/kg). To assess possible wall effects, two container depths (30 and 60mm) were tested (Figure 9b), yielding comparable results.

As mentioned before sets of 3 tests are carried out to obtain an average value at each time. The results are presented in Table 3. A total of 10 series were carried out for increasing dosages of accelerator D_{acc} (6, 9, 12 mL/kg). A_{thix} is deduced from a linear regression from Eq. 2 and the average residual \bar{R} of the measurements compared to the model is given.

The calculated A_{thix} are well repeatable and in the expected order of magnitude with an experimental uncertainty \bar{R} similar to the uncertainty $\delta\tau$ of the instrument for each vane head indicated in the Table 2. At 12mL/kg, we reach the measurement limits of the instrument, the material being too structured.



Figure 12: Photograph of a classic scissometer (Source: mtlabs.co.nz)

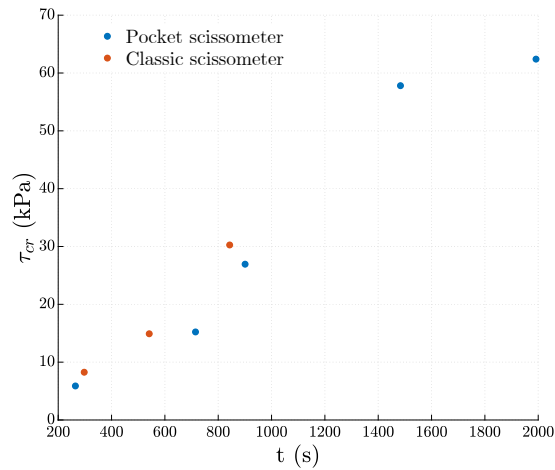


Figure 13: Benchtop measurements of shear yield stress τ_{cr} at different resting time t of the same mortar, with pocket and classic vane.

Note also the importance of the proposed prior footprint: for tests n^o 6 and 9, underlined in Table 3, damages due to blades introduction, artificially decrease the yield stress values.

The relevance of the tool being established, we propose here its use inline.

6. Inline measurement on the printed material

This section addresses the final objective of the proposal, which is to demonstrate the opportunities of the inline method. Here the material is not mixed

i_{exp}	Footprints	Vane head(s)	D_{acc} (mL/kg)	A_{thix} (Pa/s)	R (Pa)
1	no	Sensitive	6	20.3	1373
2	no	Sensitive	6	20.2	1029
3	no	Sensitive	6	16.5	1453
4	no	Sensitive + Std	6	21.6	1452
5	no	Sensitive + Std	6	20.8	3348
<u>6</u>	no	<u>Standard</u> (Std)	<u>9</u>	<u>54.2</u>	<u>6533</u>
7	yes	Standard	9	69.9	2989
8	yes	Standard	9	89.6	3003
<u>9</u>	no	<u>Standard</u>	<u>12</u>	<u>44.1</u>	<u>30000</u>
10	yes	Standard + HC	12	67.3	5393

Table 3: Experimental benchtop results with the pocket vane. Notation: i_{exp} : experiment number, D_{acc} dosage of the accelerating additive, \bar{R} mean residual of the A_{Thix} estimate. Underlined results for tests without prior footprints.

once and for all, but accelerated at the level of the extrusion head and therefore produced identically and continuously (unless the accelerator is not well dispersed which would be clearly visible because the quality of the print would be strongly degraded). If the initial non-accelerated batch (40 liters) remains within its open time (approximately 45 min), each sample is produced and tested at a given age independently of the others, allowing for better precision of each yield stress assessment by increasing the number of tests made at each given resting time t . The spacing between trials Δt_{test} is no longer constrained by the duration of the unit trial t_{min} nor by the value of the ratio $\frac{\delta\tau}{A_{thix}}$ (see Eq.6).

Before the test, the initial threshold τ_0 is estimated using the so-called slugs-test which consists to deduce the yield stress analytically from the weight of the mortar drops falling from the head nozzle (details in [23]). The steps of the protocol are previously illustrated in Figure 10 for the ex-situ condition (in a recipient), and in Figure 11 for the in-situ condition, directly on a printed wall.

6.1. Comparison between in-situ inline and ex-situ inline measurements

Let us now compare the inline results, for tests carried out on containers filled with the robot (ex-situ, Figure 9, or for printed samples (in-situ Figure 11).

The results (Figure 14) obtained using the two methods are comparable. Indeed, all the data points (ex-situ and in-situ measurements) were correlated together and the linear regression yields a coefficient of determination R^2 of 0.84 which is reasonable. The correlation results of printer-filled and printed lace measurements are shown in Table 4 showing little difference in the actual structuration rate (A_{thix}) estimation and coefficient of determination R^2 . Moreover, once again, the assumed linear evolution is demonstrated. In the Appendix, the tables 5 and 6 provide the complete set of results.

In the future, repeating more of these experiments will certainly provide enough

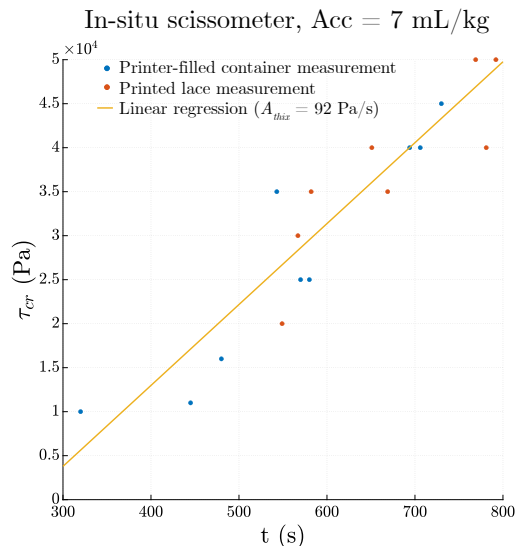


Figure 14: inline measurements of the shear stress τ_{cr} at different ages, by measuring material from a container filled (ex-situ) with the robot or directly on printed laces (in-situ).

Dataset	A_{thix} (Pa/s)	R^2
Printer-filled container measurements	91	0.86
Printed lace measurements	87	0.70
All measurements	92	0.84

Table 4: Comparison of build-up rate between ex-situ inline measurements and in-situ inline measurements.

data to quantify more precisely the dispersion between the two test conditions and eventual heterogeneities.

6.2. Comparison between benchtop and in-line measurements

This section aims to study the difference between these two approaches. The bench top test is carried out as previously described, by accelerating the mortar in a table mixer, and the fresh unaccelerated mortar is collected from the printing system so that both tests are issued from the same mortar batch. Figure 15 presents typical results obtained during this comparative bench-top and inline test campaigns.

The trend is again linear for both test types. The dispersion at a given time demonstrates the advantage of repeating 3 times the measurements as indicated in the protocol. However, the structuration rate of the printed material is much higher than that of the benchtop: the structuring rate A_{thix} of the printed material (online), $70.3Pa/s$, is 5 times higher than that of the benchtop, $14.3Pa/s$. Several hypotheses can be proposed:

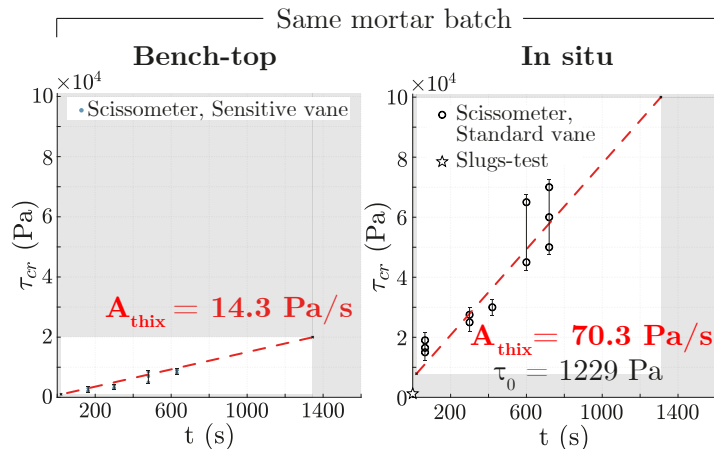


Figure 15: Time-stress graphs of inline and bench-top testing with material accelerated at a typical dosage for printing (6mL/kg). The error bars represent the interval containing the values of all measurements at a given time, plus or minus half the uncertainty δ_t of the vane head used.

- Firstly, there is the heating of the material in the pump and printing head, which may accelerate hydration reactions [37].
- Secondly, shearing inside the printing head may affect the mortar microstructure and help for good dispersion of the accelerator.

Indeed, the shear rate experienced by the mortar within the screw auger equipped on the printing head is probably higher than that of the table mixer, resulting in better deflocculation of the material and an increase of the specific surface area of the cement grains available within the cement paste. This may allow better reactivity.

It is therefore clear that a bench-made material and an inline printed material do not have the same properties. This underlines the importance of inline measurements, which are more representative and allow process-related effects to be captured.

7. Some other key figures of the method

Here we give some information about the potential and the limits of the method.

Due to the benchtop procedure and the fact that the containers are small and quickly filled, the homogeneity of the material across the tested sample (condition 8) is easily verified.

We precise the bounds t_{min} , τ_{min} , τ_{max} and t_{max} of the measurement window of this inline test. t_{min} is about 20 seconds. τ_{max} varies according to the

chosen vane head: 20, 100, or 250 kPa. For τ_{min} , the greater value between the one given by the Equation 2 for t_{min} , and the minimum threshold measurable by the vane head (Table 2), is chosen. t_{max} depends on A_{thix} and τ_{max} and is therefore also deduced from Equation 2. t_{max} may be limited not by the instrument but by the open time of the mortar, typically 45 minutes, and the volume of the batch (50L). Figure 16 represents the span of the measurement

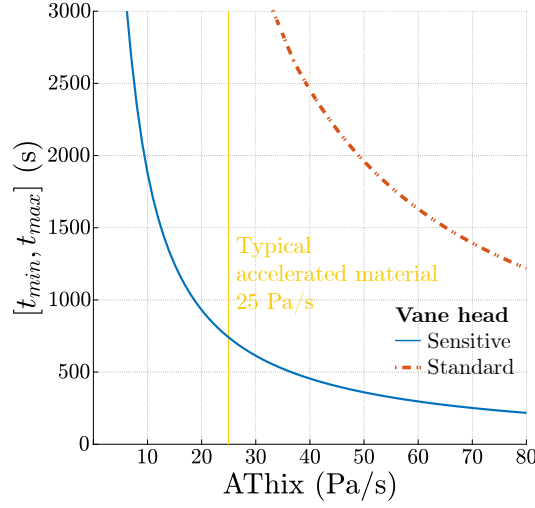


Figure 16: Measurement window size $[t_{min}, t_{max}]$ for Sensitive and Standard vane head as a function of A_{thix} with $\tau_0 = 1000Pa$.

window as a function of A_{thix} for a material with $\tau_0 = 1000Pa$, and this for two measurement vane heads (Sensitive and Standard) indicated by the blue and red curves. The curves are decreasing, because the higher A_{thix} , the faster the limit (τ_{max}, t_{max}) is reached. For $A_{thix} = 25Pa/s$, the size of the window is 750 s (12.5 min) for the Sensitive vane head and more than 45 min for the Standard vane head which is largely sufficient.

The delay between tests Δt_{test} , as we have seen (§2.4) is either t_{min} the minimum time to carry out a test, or the ratio between the precision of the instrument and the structuration rate $\frac{\delta_\tau}{A_{thix}}$. For inline situations, the tests can be sequenced and spaced freely, because the material is produced continuously. It is therefore not t_{min} which imposes the delay, but $\frac{\delta_\tau}{A_{thix}}$.

This is illustrated for the sensitive vane head (precision $\delta_\tau = 1kPa$) in Figure 17 where the continuous line curve highlighted in yellow represents the minimum value of Δt_{test} based on A_{thix} .

The evolution of the maximum achievable number of trials n_{max} as a function of A_{thix} with $\tau_0 = 1000Pa$ is illustrated in Figure 18, and follows two successive linear trends. Since n_{max} is inversely proportional to Δt_{test} , which is inversely

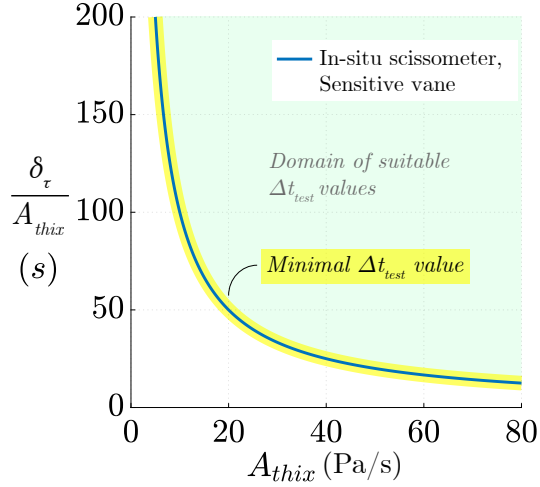


Figure 17: Δt_{test} as a function of A_{thix} for Sensitive vane head.

proportional to A_{thix} , n_{max} is proportional to A_{thix} . For the Sensitive vane head, the first part concerns structuring rates below $7.5 Pa/s$. The higher A_{thix} , the closer the trials can be to each other. The second part illustrates the limit of the τ_{max} measurement capacity of the vane head used.

At the bottom of Figure 18, we have represented the possible measurement range of A_{thix} for each vane head, that is say for $n \geq 3$. It can thus be seen that the two vane heads make it possible to theoretically measure very high structuring rates, in the range of hundred Pascals per second.

8. Conclusion

Two-component concrete 3D printing is a very promising process, permitting low power consumption at a high flow rate even for highly viscous mortar, since its yield stress remains low during the pumping. An adapted accelerator permits continuously structuring the mortar, by increasing its yield stress, from a liquid behavior to a sufficiently solid behavior, usually with a larger build-up rate than alternative processes. This allows for more complex geometries. However, it raises the question of choosing the precise dosage of accelerator that should be high enough to avoid catastrophic failure, but low enough to avoid the so-called "cold joints". An efficient measure of the build-up rate of the mortar is then really needed for efficient quality control. To do so, simple tools allowing the yield stress measurements need to be proposed and assessed, in the same trend that the so-called *Fifty-cent rheometer* concept as defined in [25]. Another question concerns the replicability of measurement made using bench-top measurement and small mortar specimens to the real material production during printing. This paper tackles those questions by introducing a new simple inline metrology for assessing the build-up rate of highly reactive mortars. For

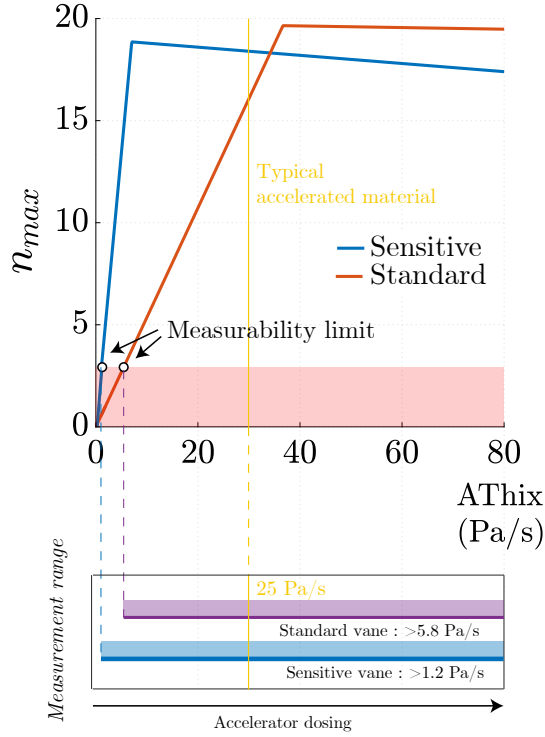


Figure 18: Number of maximum measurements n_{max} as a function of A_{thix} for the Sensitive and Standard vane heads.

this purpose, a pocket shear vane tester is tested for the first time and shown to meet the requirements and prefigure a simple online test for systematic print qualification. We demonstrate that the geometry of the pocket hand vane is more appropriate for our particular problem than classical vane geometry, since mobilizing smaller quantities of mortar, and enables in-situ shear yield stress measurements even on freshly printed layers. The various vane geometries allow for measuring the yield stress from 1kPa to 250 kPa also perfectly meeting the requirements. Original protocols are proposed and tested, and the main results can be summarized :

- The yield stress values measured using a pocket hand vane are repeatable and similar to the values obtained using a classical hand vane.
- A linear evolution of the parameter A_{thix} (see Eq.2) is relevant to model the build-up rate, i.e. the shear yield stress evolution over the first hour, for mortars accelerated using an aluminum sulfate accelerator.
- The inline build-up rate is significantly higher, up to 5 times higher than the build-up rate A_{thix} of samples prepared using a benchtop mixer.

- The build-up rate increases with higher accelerator dosage, which demonstrates the potential of the 2K strategy in adjusting material properties on the fly.
- Using the pocket vane, the shear yield stress can be directly measured on printed laces, or in recipients filled by the extrusion head.
- The pocket hand vane enables inline measurements of A_{thix} in the range of hundred Pascal per second.

To conclude the pocket hand vane appears as a good contender for a *Fifty-cent rheometer* for 2K printable micro-mortars ($\phi_{max} = 0.8mm$) and will be widely and systematically evaluated in our next printing sessions. It would provide quantitative values of the mechanical strength and their evolution that can be used for simulating the process and ensuring successful printing. Future work should also focus on the applicability of the pocket shear vane to printable concrete including larger particles.

Appendix

In this Appendix, we provide the measurement data on the printer-filled and printed lace measurement comparison (see Figure 14).

Yield stress τ_{cr} (kPa)	Age t (s)	Vane head
10	320	Sensitive
11	445	Sensitive
16	480	Sensitive
35	543	Standard
25	570	Standard
25	580	Standard
40	694	Standard
40	706	Standard
45	730	Standard

Table 5: Experimental data of printer-filled container measurements.

Acknowledgment

This work was made in the framework of Leo Demont’s Ph.D. Leo Demont’s thesis is funded by Ecole des Ponts ParisTech and [Build’in](#), a technological platform of its Co-Innovation Lab. The authors also acknowledge the fruitful collaboration with XTreeE, the technology provider of the extruder, and Jean-Michel Pereira for suggesting the use of a pocket shear vane.

Yield stress τ_{cr} (kPa)	Age t (s)
20	549
30	567
35	582
40	651
35	669
45	669
50	769
40	781
50	792

Table 6: Experimental data of printed lace measurements. The vane head used is Standard.

References

- [1] N. P. Roussel, Rheological requirements for printable concretes, 2018. doi: [10.1016/j.cemconres.2018.04.005](https://doi.org/10.1016/j.cemconres.2018.04.005).
- [2] T. Wangler, R. J. Flatt, N. Roussel, A. Perrot, M. Sonebi, R. Wolfs, F. Bos, D. Lowke, N. Freund, D. Stephan, U. Pott, L. Reiter, S. Grünewald, W. R. L. da Silva, G. De Schutter, Printable Cement-Based Materials: Fresh Properties Measurements and Control, in: N. Roussel, D. Lowke (Eds.), Digital Fabrication with Cement-Based Materials, Vol. 36, Springer International Publishing, Cham, 2022, pp. 99–136. doi: [10.1007/978-3-030-90535-4_4](https://doi.org/10.1007/978-3-030-90535-4_4).
- [3] J.-F. Caron, L. Demont, N. Ducoulombier, R. Mesnil, [3d printing of mortar with continuous fibres: Principle, properties and potential for application](#), Automation in Construction 129 (2021) 103806. doi: <https://doi.org/10.1016/j.autcon.2021.103806>.
URL <https://www.sciencedirect.com/science/article/pii/S0926580521002570>
- [4] N. Ducoulombier, L. Demont, C. Chateau, M. Bornert, J.-F. Caron, Additive Manufacturing of Anisotropic Concrete: A Flow-Based Pultrusion of Continuous Fibers in a Cementitious Matrix., Procedia Manufacturing 47 (2020) 1070–1077. doi: [10.1016/j.promfg.2020.04.117](https://doi.org/10.1016/j.promfg.2020.04.117).
- [5] L. Demont, N. Ducoulombier, R. Mesnil, J.-F. Caron, Flow-based pultrusion of continuous fibers for cement-based composite material and additive manufacturing: Rheological and technological requirements, Composite Structures 262 (2021) 113564. doi: [10.1016/j.compstruct.2021.113564](https://doi.org/10.1016/j.compstruct.2021.113564).
- [6] P. Carneau, R. Mesnil, O. Baverel, N. Roussel, Layer pressing in concrete extrusion-based 3D-printing: Experiments and analysis, Cement and Concrete Research (2022) 106741 doi: [10.1016/j.cemconres.2022.106741](https://doi.org/10.1016/j.cemconres.2022.106741).

- [7] A. Perrot, D. Rangeard, A. Pierre, Structural built-up of cement-based materials used for 3D-printing extrusion techniques, *Materials and Structures* 49 (4) (2016) 1213–1220. doi:10.1617/s11527-015-0571-0.
- [8] N. Roussel, A thixotropy model for fresh fluid concretes: Theory, validation and applications, *Cement and Concrete Research* 36 (10) (2006) 1797–1806. doi:10.1016/j.cemconres.2006.05.025.
- [9] A. Perrot, A. Pierre, S. Vitaloni, V. Picandet, Prediction of lateral form pressure exerted by concrete at low casting rates, *Materials and Structures* 48 (7) (2015) 2315–2322.
- [10] J. Kruger, S. Zeranka, G. van Zijl, An ab initio approach for thixotropy characterisation of (nanoparticle-infused) 3D printable concrete, *Construction and Building Materials* 224 (2019) 372–386. doi:10.1016/j.conbuildmat.2019.07.078.
- [11] C. Gosselin, R. Duballet, P. Roux, N. Gaudillière, J. Dirrenberger, P. Morel, Large-scale 3D printing of ultra-high performance concrete – a new processing route for architects and builders, *Materials & Design* 100 (2016) 102–109. doi:10.1016/j.matdes.2016.03.097.
- [12] V. Esnault, ONLINE CONTROL OF RHEOLOGY OF BUILDING MATERIAL FOR 3D PRINTING (Dec. 2017).
- [13] V. Esnault, A. Labyad, M. Chantin, F. Toussaint, Experience in On-line Modification of Rheology and Strength Acquisition of 3D Printable Mortars, in: T. Wangler, R. J. Flatt (Eds.), *First RILEM International Conference on Concrete and Digital Fabrication – Digital Concrete 2018*, RILEM Bookseries, Springer International Publishing, Cham, 2019, pp. 24–38. doi:10.1007/978-3-319-99519-9_3.
- [14] A. Bravo, T. Cerulli, C. Maltese, C. Pistolesi, D. Salvioni, Effects of increasing dosages of an alkali-free accelerator on the physical and chemical properties of a hydrating cement paste, *Special Publication* 217 (2003) 211–226.
- [15] I. Dressler, N. Freund, D. Lowke, The Effect of Accelerator Dosage on Fresh Concrete Properties and on Interlayer Strength in Shotcrete 3D Printing, *Materials* 13 (2) (2020) 374. doi:10.3390/ma13020374.
- [16] D. Lowke, Thixotropy of scc—a model describing the effect of particle packing and superplasticizer adsorption on thixotropic structural build-up of the mortar phase based on interparticle interactions, *Cement and Concrete Research* 104 (2018) 94–104. doi:https://doi.org/10.1016/j.cemconres.2017.11.004.
URL <https://www.sciencedirect.com/science/article/pii/S0008884617305604>

- [17] L. Reiter, T. Wangler, N. Roussel, R. J. Flatt, The role of early age structural build-up in digital fabrication with concrete, *Cement and Concrete Research* 112 (2018) 86–95. doi:[10.1016/j.cemconres.2018.05.011](https://doi.org/10.1016/j.cemconres.2018.05.011).
- [18] R. J. M. Wolfs, F. P. Bos, T. A. M. Salet, Correlation between destructive compression tests and non-destructive ultrasonic measurements on early age 3D printed concrete, *Construction and Building Materials* 181 (2018) 447–454. doi:[10.1016/j.conbuildmat.2018.06.060](https://doi.org/10.1016/j.conbuildmat.2018.06.060).
- [19] S. Amziane, A. Perrot, T. Lecompte, A novel settling and structural build-up measurement method, *Measurement Science and Technology* 19 (10) (2008) 105702. doi:[10.1088/0957-0233/19/10/105702](https://doi.org/10.1088/0957-0233/19/10/105702).
- [20] H. Sleiman, A. Perrot, S. Amziane, A new look at the measurement of cementitious paste setting by Vicat test, *Cement and Concrete Research* 40 (5) (2010) 681–686. doi:[10.1016/j.cemconres.2009.12.001](https://doi.org/10.1016/j.cemconres.2009.12.001).
- [21] D. Lootens, Ciments et suspensions concentrees modeles. Ecoulement, encombement et floculation., Ph.D. thesis.
- [22] R. Nicolas, B. Richard, D. Nicolas, I. Irina, K. J. Temitope, L. Dirk, M. Viktor, M. Romain, P. Arnaud, P. Ursula, R. Lex, S. Dietmar, W. Timothy, W. Rob, Z. Wenqiang, Assessing the fresh properties of printable cement-based materials: High potential tests for quality control, *Cement and Concrete Research* 158 (2022) 106836. doi:[10.1016/j.cemconres.2022.106836](https://doi.org/10.1016/j.cemconres.2022.106836).
- [23] N. Ducoulombier, R. Mesnil, P. Carneau, L. Demont, H. Bessaies-Bey, J.-F. Caron, N. Roussel, The “Slugs-test” for extrusion-based additive manufacturing: Protocol, analysis and practical limits, *Cement and Concrete Composites* 121 (2021) 104074. doi:[10.1016/j.cemconcomp.2021.104074](https://doi.org/10.1016/j.cemconcomp.2021.104074).
- [24] Bartos, M. Sonebi, Tamimi, *Workability and Rheology of Fresh Concrete: Compendium of Tests*, 2002.
- [25] N. Roussel, P. Coussot, “Fifty-cent rheometer” for yield stress measurements: From slump to spreading flow 15.
- [26] J. J. Assaad, J. Harb, Y. Maalouf, Measurement of yield stress of cement pastes using the direct shear test, *Journal of Non-Newtonian Fluid Mechanics* 214 (2014) 18–27. doi:[10.1016/j.jnnfm.2014.10.009](https://doi.org/10.1016/j.jnnfm.2014.10.009).
- [27] Z. Toutou, N. Roussel, C. Lanos, The squeezing test: A tool to identify firm cement-based material’s rheological behaviour and evaluate their extrusion ability, *Cement and Concrete Research* 35 (10) (2005) 1891–1899. doi:[10.1016/j.cemconres.2004.09.007](https://doi.org/10.1016/j.cemconres.2004.09.007).
- [28] A. Rahul, M. Santhanam, H. Meena, Z. Ghani, *3d printable concrete: Mixture design and test methods*, *Cement and Concrete Composites* 97 (2019) 13–23. doi:<https://doi.org/10.1016/j.cemconcomp.2018.12.014>.

URL <https://www.sciencedirect.com/science/article/pii/S0958946518303275>

- [29] ASTM, Standard Test Method for Approximating the Shear Strength of Cohesive Soils by the Handheld Vane Shear Device, https://www.astm.org/d8121_d8121m-18.html (2019).
- [30] S. Austin, P. Robins, C. Goodier, Workability, Shear Strength and Build of Wet-Process Sprayed Mortars, Loughborough University, 1999.
- [31] N. Roussel, F. Cussigh, Distinct-layer casting of SCC: The mechanical consequences of thixotropy, *Cement and Concrete Research* 38 (5) (2008) 624–632. doi:10.1016/j.cemconres.2007.09.023.
- [32] A. F. Omran, Portable Vane Test to Assess Structural Buildup at Rest of Self-Consolidating Concrete, *ACI Materials Journal* 108 (6) (2011). doi:10.14359/51683466.
- [33] L. Cadling, S. Odenstad, Vane Borer. An Apparatus for Determining the Shear Strength of Clay Soils Directly in the Ground, Statens geotekniska institut, 1950.
- [34] M. Keentok, J. F. Milthorpe, E. O'Donovan, On the shearing zone around rotating vanes in plastic liquids: Theory and experiment, *Journal of Non-Newtonian Fluid Mechanics* 17 (1) (1985) 23–35. doi:10.1016/0377-0257(85)80003-3.
- [35] N. Q. Dzuy, D. V. Boger, Direct Yield Stress Measurement with the Vane Method, *Journal of Rheology* 29 (3) (1985) 335–347. doi:10.1122/1.549794.
- [36] D. Boger, Rheology and the Minerals Industry, *Mineral Processing and Extractive Metallurgy Review* 20 (1) (2000) 1–25. doi:10.1080/08827509908962460.
- [37] B. Lothenbach, F. Winnefeld, C. Alder, E. Wieland, P. Lunk, Effect of temperature on the pore solution, microstructure and hydration products of Portland cement pastes, *Cement and Concrete Research* 37 (4) (2007) 483–491. doi:10.1016/j.cemconres.2006.11.016.